ISSN 1946-7664. MCFNS 2020
Vol. 12, Issue 1, pp. 1–15
Mathematical and Computational Forestry & Natural-Resource Sciences

AVAILABLE ONLINE AT HTTP://MCFNS.COM

Submitted: Oct. 3, 2019
Accepted: Dec. 6, 2019
Published: Mar. 30, 2020
Last Correction: Feb. 4, 2020

AN INTEGRATED SYSTEM FOR ESTIMATING FOREST BASAL AREA FROM SPHERICAL IMAGES

H. Wang , J.A. Kershaw , T. Yang , Y. Hsu , X. Ma , Y. Chen

University of New Brunswick, The Faculty of Forestry and Environmental Management, Fredericton, NB, Canada

Abstract. Basal area is one of the most important parameters in forest inventory, but data collection by traditional methods is often time consuming and labor intensive. This study uses a new, portable, and relatively inexpensive 360° spherical camera to estimate stand basal area and make permanent digital forest records. Forty-five plots in Newfoundland and eighty-three plots in New Brunswick were used to compare traditional field inventory with spherical photo inventory and to analyze potential factors impacting results. Results showed that (1) photo-estimated basal area is similar to traditional methods measured by diameter tape and fixed-area plots or by angle gauge counting; (2) better accuracy and precision can be achieved when adding multiple digital sample locations to avoid effects of hidden trees caused by nearby trunks; (3) understory tree and shrub density did not significantly influence stem visibility; and (4) differences among different users were tested and shown to not be significant. An open-source software package was developed to make the implementation of our technique easy and efficient.

Keywords: panorama images; digital camera; forest inventory; remote sensing; horizontal point sampling

1 Introduction

Forests are the dominant terrestrial ecosystem on Earth and account for three quarters of the gross primary productivity of the biosphere and about 80% of plant biomass (Pan et al., 2013). In addition to ecosystem services like watershed protection and carbon storage (Chazdon, 2008), the other economic and social products provided by forests are of great interest to land owners and forest managers (Christensen et al., 1996; Gillis, 1990). To satisfy the multiple demands from forests, advanced tools used to collect data efficiently are required for making good forest management decisions (Baskerville, 1986; Bettinger et al., 2017; Clutter et al., 1983). Therefore, coupling advanced technology with traditional forest inventories to save costs and time, and to improve accuracy of estimates, are of great importance (Husch, 1980; Iles, 2003; Kershaw et al., 2016).

Forest inventories typically collect measurements on individual trees (e.g., species, diameter at breast height, and total height) and use these measures to estimate stand-level parameters such as density, volume, and biomass (Kershaw et al., 2016). Stand basal area, defined as the sum of individual tree cross-sectional areas, is one of the most common stand-level parameters estimated in most forest inventories (Iles, 2003; Kershaw et al., 2016). Basal area is often expressed at breast height (1.3 m in SI and 4.5 ft in the Imperial system). Basal area is an important measure of stand density that incorporates tree size as well as number (Kershaw et al., 2016). It is a fundamental component of volume and biomass calculations (Iles, 2003; Jenkins et al., 2003; Kershaw et al., 2016; Lambert et al., 2005; Slik et al., 2010) and is an important stand characteristic for forest growth models (Lootens et al., 2007; Opie, 1968; Weiskittel et al., 2011).

When using fixed-area sampling units, basal area is calculated from individual tree diameter measurements (Kershaw et al., 2016), which can be a time consuming endeavor depending upon tree density and sampling unit size. Angle count sampling (Bitterlich, 1947, 1984; Iles, 2003), or horizontal point sampling as it is commonly known (Bitterlich, 1984; Grosenbaugh, 1952; Iles, 2003; Kershaw et al., 2016), is an alternative method that measures basal area by counting trees that subtend (i.e., appear as large or larger than) a projected angle and multiplying by the basal area expansion factor (BAF). The ability to estimate basal area by counting trees makes angle count sampling a very efficient sam-

pling approach (Bitterlich, 1984; Iles, 2003; Kershaw et al., 2016; Marshall et al., 2004; Yang et al., 2017).

DeCourt (1956) was the first to recognize that it was possible to conduct angle count sampling using photographs. Grosenbaugh (1963) hinted at this application but did not develop the technique very deeply. Because of the time and costs associated with film-based imagery, photo-based angle count sampling was not developed any further until the work by Stewart et al. (2004) who proposed photo-based angle count sampling using 8 directional photos and developed methods to correct for image distortion near the photo edges. Dick (2012), using panoramic stitching software, merged 24 images into a single panorama image and eliminated the need for distortion correction. By defining an angle gauge in terms of pixels, Dick (2012) developed a simple photographic angle count method implemented in ArcGIS (ESRI, Redlands, CA). Independently, Fastie (2010) merged 504 images into an ultra-high resolution panorama to estimate basal area. Given that angle count sampling was already an extremely efficient inventory system in the field, these approaches for photo-based sampling were more curiosities than operational developments.

The main advantage of the photo-based method was that basal area estimates could potentially be extracted from archive photos (Stewart et al., 2004). However, photo-based approaches also suffered from potential under-estimation bias due to occluded (hidden) trees (Dick, 2010; Zasada et al., 2013). In addition to the hidden trees, other potential impacts such as understory vegetation, counting dead trees, image resolution, and user errors were not systematically explored in these previous studies.

Digital technology continues to advance rapidly and stitching packages are now available on many smart phones. In addition, the recent development of consumer-grade spherical cameras opens the opportunity to obtain panoramic photos from single exposures controlled by a smart phone. The ability to rapidly obtain panoramic photos and develop onboard processing creates an opportunity to revisit the photo-based angle count sampling idea. The goal of this study was to develop an open-source software package that implements angle count sampling using spherical photos taken from a Ricoh Theta S, which is a relatively inexpensive consumer-grade camera. The specific objectives were: (1) to derive the geometry of applying the angle-count sampling idea to spherical images to obtain basal area estimates; (2) to assess the precision and accuracy of this approach compared to traditional field measured data; (3) to assess the inter-observer variability in implementing this approach; and (4) to assess the effects of understory tree density on the photo-based estimates.

2 Methods and Materials

2.1 Study Sites

Data for this study come from two different studies. The first study was three early spacing trials located in western Newfoundland (NL). The NL sites were located in the Boreal Forest region (Rowe, 1972) and were dominated by balsam fir (*Abies balsamea*) with some black spruce (*Picea mariana*) and other boreal species. The trials were established in the early 1980's. At each site, there were three replicates of five thinning spacing treatments: Control (no spacing), 1.2 m, 1.8 m, 2.4 m, and 3.0 m average spacing.

The second study was located on the Noonan Research Forest (NRF) in central New Brunswick, Canada, managed by the University of New Brunswick. The NRF was located in the Acadian Forest region (Rowe, 1972), and was composed of a variety of stand types from relatively pure coniferous stands to mixed hardwood-softwood stands. A permanent 100 m by 100 m inventory sample grid was overlaid on the NRF in 1999. The 83 grid intersections within the Femelschlag Research Study were used in this study.

2.2 Data Collection

2.2.1 Field Data

Only the most recent measurements of the 45 NL plots (3 trials × 5 treatments/trial × 3 replicates/treatment) were used in this study (Tab. 1). Plot sizes varied by treatment with the goal to have approximately 100 trees per plot at the initial measurement. The plot radii were: Control (no spacing) = 5.2 m; 1.2 m spacing = 7.2 m; 1.8 m spacing = 10.4 m; 2.4 m spacing = 15.0 m; and 3.0 m spacing = 18.0 m). On each plot, all trees taller than 1.3 m were measured for diameter at breast height (DBH, 1.3 m above ground, nearest 0.1 cm) and total height (nearest 0.1 m). Field basal area (FBA, m^2/ha) was calculated using:

$$\mathrm{FBA} = \mathrm{ExpF} \times \sum_{i=1}^{n} \left(\pi \left(\frac{DBH_i}{200} \right)^2 \right) \qquad (1)$$

where ExpF is the plot expansion factor (ExpF=$10000/(\pi R^2)$; R is plot radius in meters).

On the NRF sample points, a 2M BAF (basal area factor; i.e., each tree tallied represented 2 m^2/ha basal area) angle count sample was conducted centered at the 83 grid intersections in summer 2018. All trees that subtended the projected angle were counted and FBA (m^2/ha) was calculated by multiplying the number of count trees by the BAF (2 in this case). In addition, those trees with DBHs smaller than 6 cm were tallied as understory trees by height status (less than or greater

Table 1: Average stand-level estimates (standard errors in parentheses) by trial and treatment for the 3 early spacing trials located within western Newfoundland.

Trial	Year	Treatment	Stand-Level Averages (Standard Errors)							
			Trees (num/ha)		Basal Area (m^2/ha)		DBH (cm)		Total Height (m)	
Cormack	2013	no spacing	9974	(1807)	62.39	(6.26)	8.97	(0.42)	9.21	(0.92)
		1.2m spacing	6239	(740)	49.94	(9.49)	10.14	(1.60)	8.86	(1.63)
		1.8m spacing	2978	(433)	34.41	(10.88)	12.07	(1.64)	8.73	(1.61)
		2.4m spacing	1432	(168)	32.38	(3.81)	16.98	(0.59)	10.62	(0.54)
		3.0m spacing	965	(62)	21.54	(0.92)	16.86	(0.18)	9.62	(0.23)
Pasadena	2013	no spacing	6112	(2049)	61.04	(9.36)	11.52	(1.27)	9.83	(0.82)
		1.2m spacing	3616	(863)	67.22	(5.07)	15.59	(1.95)	11.37	(1.38)
		1.8m spacing	2611	(309)	53.59	(7.29)	16.16	(0.16)	10.81	(0.43)
		2.4m spacing	1793	(545)	46.18	(10.12)	18.26	(0.86)	11.35	(0.29)
		3.0m spacing	1111	(61)	36.88	(3.04)	20.55	(0.58)	11.60	(0.33)
Roddickton	2017	no spacing	12775	(2101)	73.19	(8.06)	8.59	(0.88)	7.07	(0.62)
		1.2m spacing	4987	(1066)	54.62	(4.61)	11.94	(1.47)	8.28	(1.28)
		1.8m spacing	2927	(247)	40.58	(2.86)	13.30	(0.50)	7.94	(0.25)
		2.4m spacing	2119	(253)	40.40	(9.13)	15.50	(0.85)	8.74	(0.67)
		3.0m spacing	1253	(87)	31.25	(2.21)	17.83	(0.41)	9.12	(0.35)

than 1.3 m tall) on a 4 m radius plot centered on the grid intersections. Species and status (live or dead) also were recorded for all understory trees.

2.2.2 Digital Sample Points

For each NL sample plot, three digital sample locations were established at half the plot radius along azimuths of 120°, 240°, and 360° relative to plot center (Fig. 1.a). On the NRF sample points, only one digital sample location was established at the grid intersection (Fig. 1.a).

A Ricoh Theta S (Ricoh, 2016) spherical camera was used to capture spherical images. A single spherical image was captured at 1.6m above the ground at each digital sampling point (Fig. 1.b) and downloaded to a smart phone. Though the spherical camera records a 360° spherical image, the spherical image is projected into a 2D digital image using cylindrical projection. In this projection system, the vertical coordinate in the 2D image and related vertical angle (latitude) in spherical coordinates are always consistent no matter how far an object is from horizontal center. The image resolution was 5376 pixels in width and 2688 pixels in height.

2.3 Image Processing Software

Angle count sampling (Bitterlich, 1947, 1984) is a sampling method that uses a horizontally projected angle to select trees for inclusion in the sample (Fig. 2.a). A basal area expansion factor (BAF) is derived from the

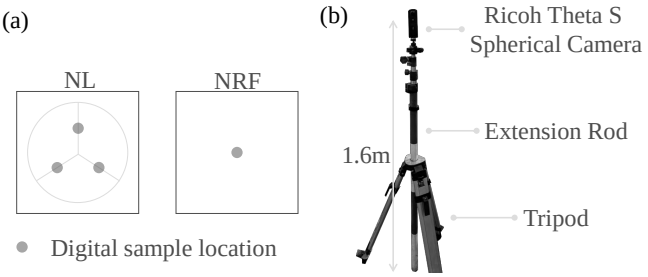

Figure 1: Digital data collection methods: (a) Digital sample location design for Newfoundland (NL) and Noonan Research Forest (NRF) (Three locations were established at the midpoint of plot radius along azimuths of 120°, 240°, and 360° in each NL plot, while only one location was set in the center for each NRF plot); (b) tripod and camera set up for spherical image acquisition.

sampling geometry associated with a tree that is at its limiting distance (Fig. 2.b). Angle count sampling is a form of sampling with variable probability and is an application of selecting sample trees based on probability proportional to size (Grosenbaugh, 1958; Kershaw et al., 2016). Basal area per ha is obtained by counting selected trees and multiplying by the BAF (Bitterlich, 1947; Kershaw et al., 2016). The key point in applying this sampling method on a spherical image was determining which trees in an image should be counted or not. In this study, two different methods for photo angle count sampling were developed and compared.

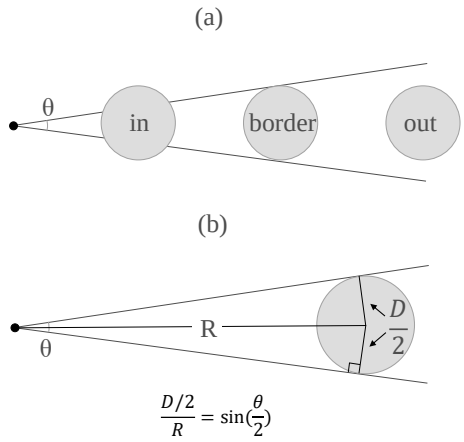

Figure 2: Sample geometry. For angle count sampling: (a) overhead view showing "in", "border" and "out" trees (gray circles represent tree trunks); (b) the relationship between horizontal angle (θ), tree diameter (D) and plot (inclusion zone) radius (R). The BAF determines the fixed horizontal angle θ which was used as the threshold to determine tree status on the spherical images.

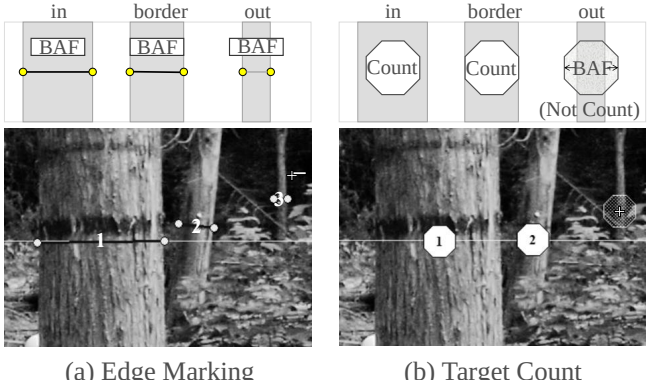

(a) Edge Marking (b) Target Count

Figure 3: Two image processing methods: (a) Edge marking method: users click on the edges of each tree. A reference bar (the length is based on BAF=1) is used to guide users so that every tree does not have to be marked; the line color indicates tree status based on desired BAF: black = "in", gray = "out"); (b) Target count method: a transparent reference octagon, scaled to the desired BAF, is provided to mark "in" trees, "out" trees are those trees smaller than the octagon target and are not marked.

2.3.1 Edge Marking Method

In this method, the horizontal angle of each individual tree trunk at breast height (1.3 m) in the image was determined (Fig. 2.b). This was accomplished by having the user mark the edges of each tree on the image (Fig. 3.a).

The width of each tree trunk was used to calculate the maximum BAF threshold (maxBAF) at "border" condition using the following equation:

$$\text{maxBAF} = \left(100 \cdot sin\left(\frac{TW}{PW} \cdot 360°\right)\right)^2 \qquad (2)$$

where TW was the pixel width of the marked tree; and PW was the total width of the spherical image (PW = 5376 in this study).

By calculating maxBAF, the number of count trees was simply the number of marked trees where maxBAF $\geqslant$ desired BAF, and photo basal area (PBA, m^2/ha) was:

$$\text{PBA} = \text{BAF} \cdot count(\text{maxBAF} \geqslant \text{BAF}) \qquad (3)$$

2.3.2 Target Count Method

This method was similar to the field angle gauge process. The software projected a horizontal angle based on the given BAF onto each tree (Fig. 3.b). To better visualize the cross-sectional angles of leaning trees, an octagon shaped target was used as the target threshold. A tree equal to or greater than the octagon target in size was marked as an "in" tree, otherwise that tree was considered an "out" tree and not counted. The PBA of this image was equal to the given BAF multiplied by the count of "in" trees.

2.3.3 Software Implementation

An open source software package, Panorama2BasalArea, was developed in Python 3.6 (Guido, 2018) to implement the angle count sampling workflows described above. It included the plot photo management, tree trunk edge marking and octagon threshold counting, individual tree management, and PBA data export (Fig. 3). When using the edge marking method, a reference scale bar was provided. Trees which were narrower than the reference scale bar (BAF=1) were ignored in order to reduce the workload associated with edge marking (Fig. 3.a). For the target marking method, a reference octagon scaled to a given BAF was provided. Only those trees equal to or larger than the reference octagon were marked (Fig. 3.b). The source code for this software package can be downloaded from: `https://github.com/HowcanoeWang/Panorama2BasalArea`. It was also packaged as an executable app for Windows platforms: `https://github.com/HowcanoeWang/Panorama2BasalArea/releases`.

2.4 Data Analysis

2.4.1 Influence of Number of Digital Sample Points

Hidden trees blocked by closer trees or understory vegetation create a potential for underestimating PBA. One possible way to deal with the hidden tree problem was to use multiple sample points in one plot. While hidden trees result in underestimation, errors in marking tree edges and judging octagon thresholds could result in over- or under-estimation relative to field basal area (FBA). To test the influence of multiple digital sample points and the effects of two tree marking methods on PBA estimates, three separate analyses were undertaken: (1) PBA estimated from one central digital sample point on the 83 NRF sample points; (2) PBA estimated on the NL plots using three individual (off-center) digital sample points; and (3) PBA estimated from the average of the three digital sample points on each NL plot. For each analysis, a simple linear regression was fitted to the FBA – PBA data:

$$\text{FBA} = b_0 + b_1 \cdot \text{PBA} \tag{4}$$

If PBA was the same as FBA, then $b_0 = 0$ and $b_1 = 1$. The resulting parameter estimates were tested for these values using t-tests and Bonferroni-adjusted alpha levels (Zar, 2009).

2.4.2 Influence of Choice of BAF

As BAF increases, the distance a tree of a certain diameter can be from plot center decreases (Fig. 2). The expected number of count trees also decreases. Both factors should result in a lower probability of hidden trees (i.e., fewer hidden trees). On the other hand, as photo BAF increases so does variation between sample points. The trade-off becomes one of under-estimation versus increased sampling error. The optimal compromise is to use a BAF that reduces the number of hidden trees without appreciably increasing sample variation. To test this idea, BAFs ranging from 2 to 15 were applied to calculate PBA, and then compared to FBA using the edge marking method (edge marking was used because the user only needs to mark trees once to determine all BAFs, whereas target counting requires multiple runs through the images). The difference between FBA and PBA were compared using bean plots, and variance and bias were visually analyzed.

2.4.3 Inter-Observer Variation

To examine inter-observer variability, 15 images from the three NL sites (one replicate from each trial) and 5 images from the NRF plots were selected as test images. These 20 images were used for the edge marking method. For the target count method, horizontally mirrored images were used. In total, there were 40 test images given to 7 individuals. Everyone had different random orders for these images. The volunteers were trained how to use the software in both modes and then instructed to mark each image in the order given. Inter-observer differences between PBA and FBA at BAF=2 for both modes were tested using linear mixed effects (LME) models. The fixed effects were PBA (covariate) and marking mode, whereas the random effects included the observer and image order.

2.4.4 Effects of Understory Density

Understory vegetation may limit sight distances in the field as well as in photos. In the field there are a variety of techniques the field observers can use to determine tree count when visibility is low. On photos, these options are not available. To test whether understory vegetation influenced PBA estimates, the difference between FBA and PBA (FBA – PBA) was graphed versus understory density, and a locally weighted scatterplot smoothing (LOWESS) regression was used to assess trends in differences over understory density. Understory density was separated into two height classes: HT $\leq$ 1.3 m and HT $>$ 1.3 m, and evaluated by height class and total understory density.

3 Results

3.1 Influence of different digital sample locations

Figure 4 shows the relationship between FBA and PBA by tree marking method and digital sample location type. With the exception of edge marking with three individual digital sampling points (Tab. 2 (e)), all slope coefficients (b_1) were not significantly different from 1.0, indicating that photo bias does not increase with increasing basal area. Results were not as consistent when examining the intercept terms. For both marking methods, when using a single digital sample location at plot center (Tab. 2 (a) and (d)), the intercept values were significantly different from 0 and almost double the intercept values (b_0) obtained using multiple digital sampling points. For the multiple digital sampling points, only the intercept term for edge marking was significantly different from 0 (Tab. 2 (e)). Both intercepts for the average of three digital sampling points were negative, though not significantly different from 0 (Tab. 2 (c) and (f)).

In terms of goodness of fit, the edge marking techniques generally had higher r^2 values and lower root mean square error (rMSE) values, indicating a stronger linear relationship between FBA and PBA (Tab. 2). All

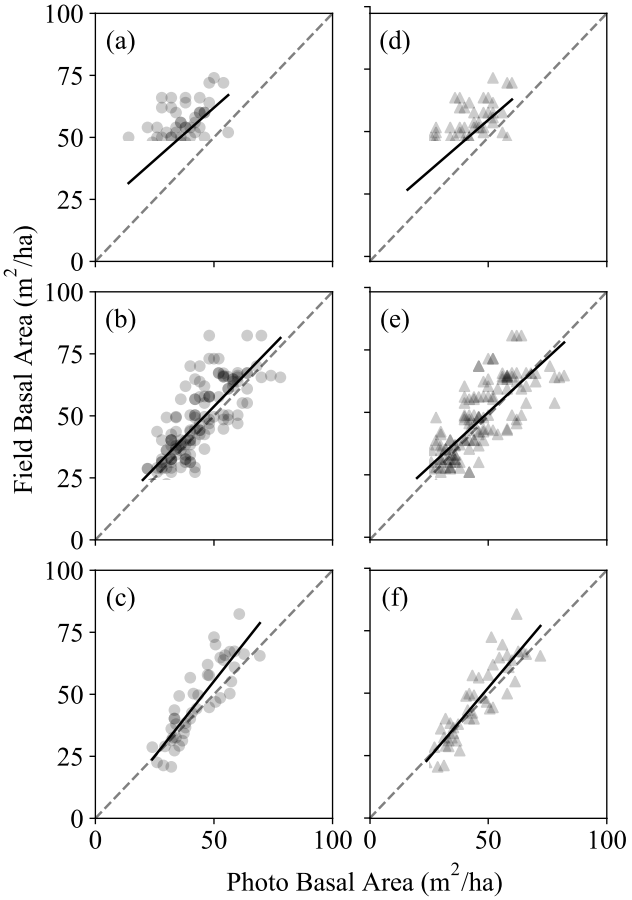

Figure 4: Comparisons between photo-estimated basal area (PBA) and field measured basal area (FBA) by digital sample location type (one center versus three individuals versus mean of three individuals) and two tree marking methods (target counting (left panels) versus edge marking (right panels)). The one center estimates (a and d) were from the Noonan Research Forest (NRF), whereas the three estimates per plot (b and e) and mean of three estimates (c and f) were from the Newfoundland (NL) spacing trials.

regressions indicate an under-estimation of FBA, except at the very lowest FBA values, when averaging across multiple digital sampling points. Under-estimation was consistent with the hypothesis of visibility bias resulting from occluded (hidden or missing) "in" trees. It was expected that the visibility bias would increase with increasing FBA; however, that was not generally observed in this study (Tab. 2 and Fig. 4).

3.2 Effects of BAF Choice

It was hypothesized that increasing BAF would result in fewer hidden trees and less user error in marking edges, and that PBA would become closer to FBA; however, that was not what was observed in this study. Figure 5 shows the effects of increasing BAFs on PBA estimation. For the NRF plots, the mean differences between FBA and PBA decreased slightly, but remained positive (indicating underestimation) across all levels of BAF. For the NL plots, the deviations decreased, but were essentially 0 across all levels of BAF. The NRF only had one central digital sample location, while NL had three sample locations (Fig. 1.a). The additional digital sample points capture a greater range of the plot variation and reduce the effects of hidden trees. One issue noted on several of the NRF plots was the presence of a tree very close to plot center. Large trees can block significant view angles on plots. Increasing BAF does not compensate for these situations. On the other hand, multiple digital sample locations minimized these effects by locating the camera at different positions within the plot.

For both NRF and NL sites, variation in the differences between FBA and PBA increased with increasing BAF (Fig. 5). Smaller plots are inherently more variable, and this was an expected outcome. It was expected that there would be an optimal BAF that minimized differences without substantial increases in variation. This was not observed in this study. It should be noted that this inference was only based on the edge marking method because of the ease of changing BAF (edges only have to be marked once to determin all BAFs). Results for target counting were not undertaken because counts would have to be made independently for each BAF tested, requiring a significant increase in image processing time.

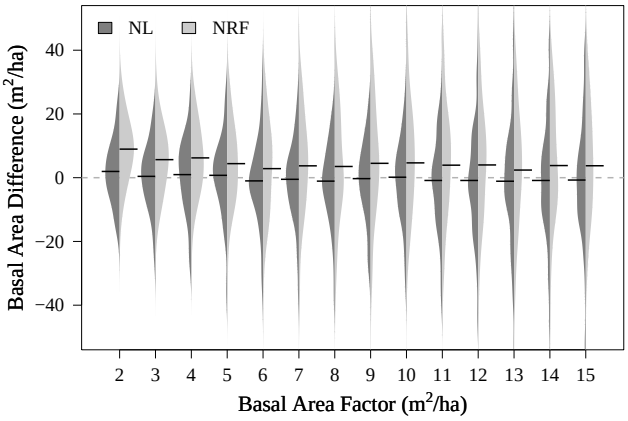

Figure 5: The influence of photo basal area factor (BAF) choice on the basal area differences (field basal area – photo basal area, m^2/ha) for Newfoundland (NL) and Noonan Research Forest (NRF). The black solid line is the mean for each location and the gray dashed line indicates perfect fit.

3.3 Inter-observer consistency

Comparisons between FBA and PBA across the seven volunteers are shown in Figure 6. Most users consistently underestimated FBA with both marking methods, with edge marking resulting in greater underestimation than target counting (Fig. 6, Column 1). While differences between users were observed (Fig. 6, Columns 2-7), on average, user estimates were comparable (i.e., LOWESS lines were very close to the 1:1 line). Target counting was generally more consistent than edge marking among different users and generally resulted in similar estimates across users (Fig. 6).

Figure 7 shows the two plots with the least and greatest deviations between users. For the least deviation plot, though different users did not mark exactly the same points across different trees, the edge positions, as well as the dark gray targets for "in" trees, were almost identical across users. The simple forest structure facilitates tree marking and results in lower variability between users. However, it was a different story for the plot with the greatest deviations. Neither the "out" trees nor the "in" trees have similar positions. Trees were very dense with smaller diameters, resulting in many "border" trees: small deviations in edge marking resulted in changes in "in" and "out" status. This problem was further compounded by the fact that edges of each tree were difficult to distinguish.

To statistically assess the effects of tree marking methods, different users and image order (i.e., familiarity with using the software), a linear mixed effects (LME) model was fitted to the data. The full model was:

$$\text{FBA} = \text{PBA} + \text{Marking} + (\text{User}) + (\text{Order}) + e \quad (5)$$

where (User) and (Order) indicate random effects. A backwards selection method was used to test significance of random effects. For the full model, the standard deviations associated with the random effects were: 2.1879

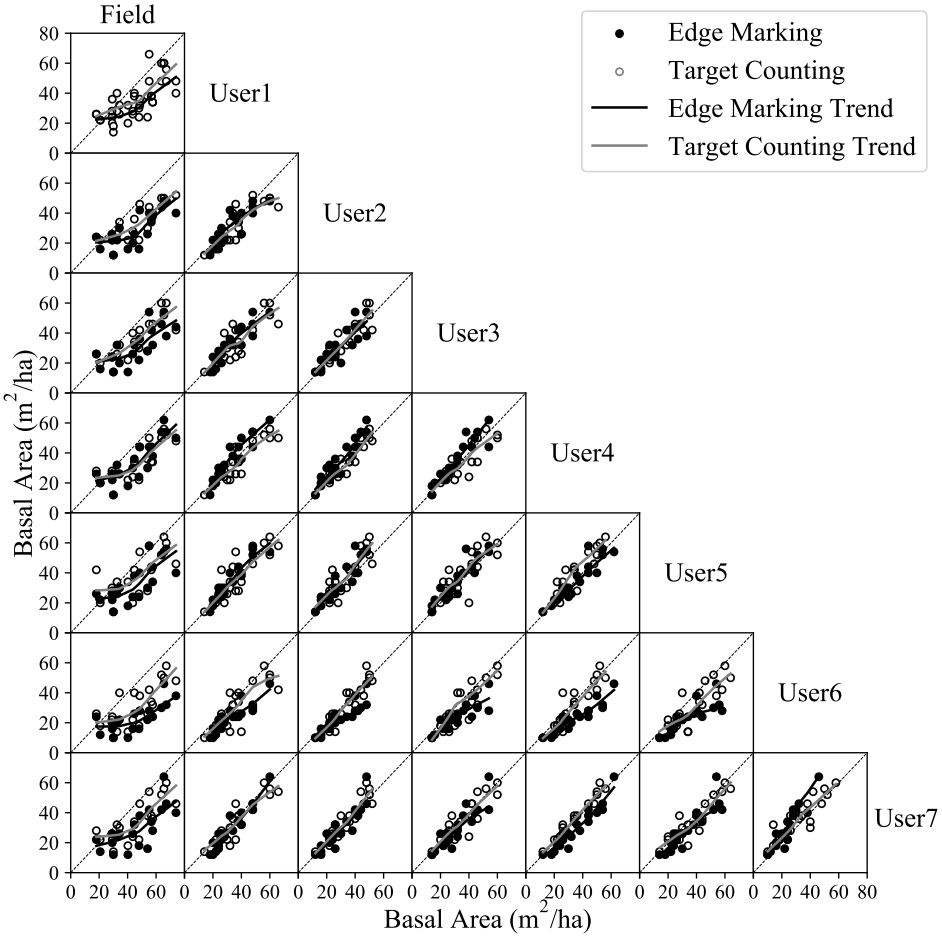

Figure 6: Comparisons between field basal area and photo basal area by two marking methods (edge marking versus target counting) among seven different users. The locally weighted scatterplot smoothing (LOWESS) regression lines show the trends between field measure and photo.

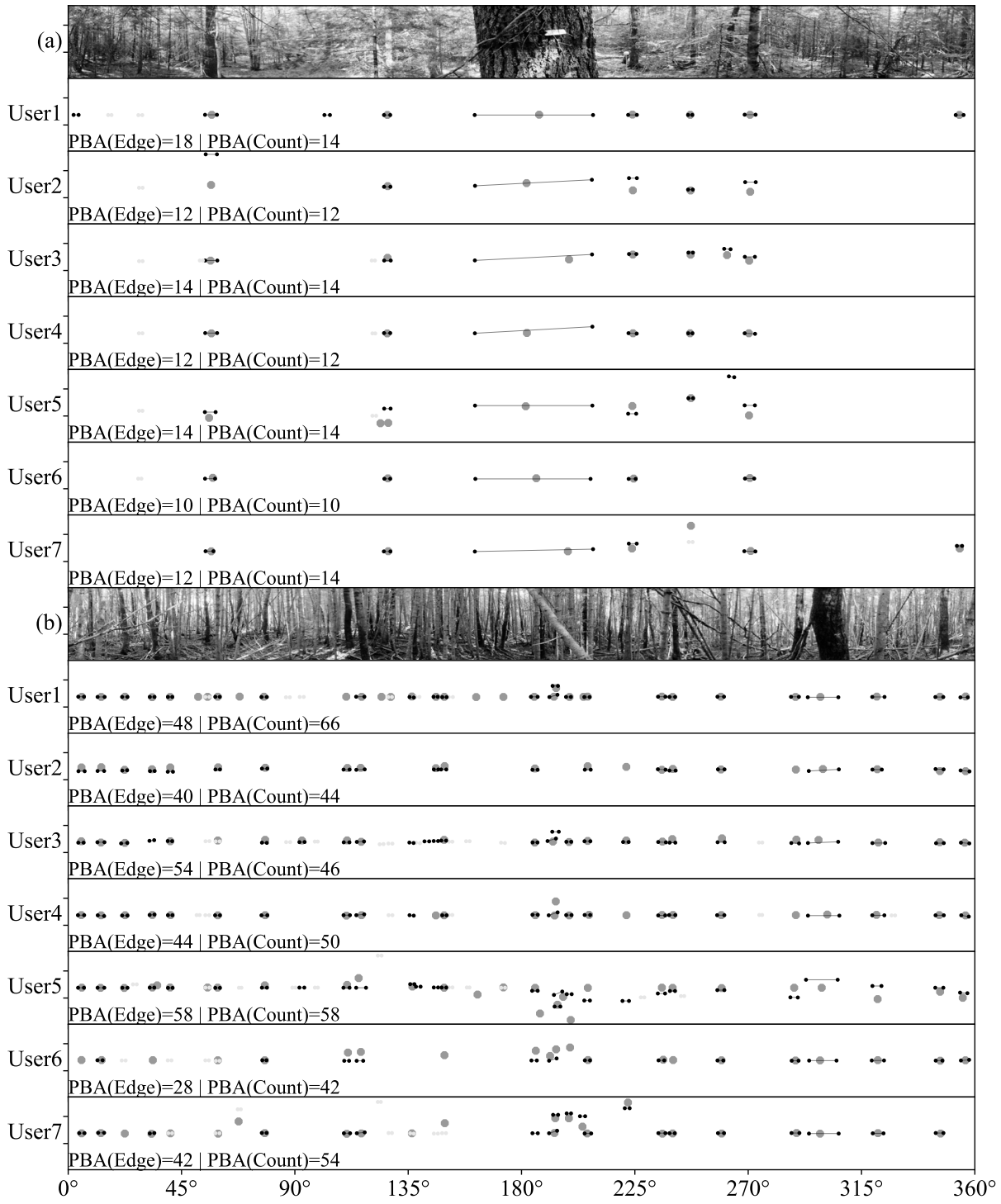

Figure 7: Two plots with the smallest (a) and largest (b) variance among seven users by two tree marking methods (edge marking versus target counting). PBA means photo-based basal area and FBA means field-based basal area. The FBA of (a) is 30 m^2/ha, and FBA of (b) is 55.2 m^2/ha. The small dots are the tree edges that users marked. The black small dot with connected lines means this tree is counted as an "in" tree, while the light gray small dots means it is an "out" tree in edge marking mode. The dark gray octagon is the "in" tree marked in target counting mode.

Table 2: Simple linear regression results for field basal area versus photo basal area by digital sample point type. The linear model is FBA=b0 + b1*PBA, if PBA is the same as FBA, then b0=0 and b1=1

Photo marking mode	Digital sample points type	Parameters	Estimate	Standard Error	p-value	r^2	rMSE
Target Counting	(a) One center estimate	b0	19.74	3.85	<0.001	0.41	9.27
		b1	0.84	0.11	0.150		
	(b) Three individual estimates	b0	4.44	3.08	0.152	0.61	9.66
		b1	0.99	0.06	0.868		
	(c) Mean of three estimates	b0	-5.22	4.79	0.282	0.75	7.77
		b1	1.21	0.11	0.063		
Edge Marking	(d) One center estimate	b0	15.69	4.09	<0.001	0.44	9.00
		b1	0.83	0.10	0.093		
	(e) Three individual estimates	b0	7.34	2.91	0.013	0.60	9.72
		b1	0.88	0.06	0.048		
	(f) Mean of three estimates	b0	-4.04	4.32	0.355	0.78	7.30
		b1	1.13	0.09	0.158		

for User and 0.7292 for Order (residual standard error was 3.7051). The model was refitted with Order excluded and a log likelihood test performed. The p-value associated with dropping Order was 0.926, indicating that image order was not a significant random effect influencing deviations from FBA. Similarly, User was subsequently dropped, and the p-value was 0.081. So, while more significant than image order, differences between users were still not significant at $\alpha = 0.05$. The final reduced model only included the fixed effects PBA (covariate) and Marking (method). Both factors were significant: PBA ($p < 0.001$) and Marking ($p < 0.01$). The root Mean Square Error was 10.6129 and the F-value associated with PBA was 320.87 ($p < 0.001$) and for Marking Method was 9.913 ($p = 0.002$).

3.4 Understory density effects

Effects of understory density on PBA estimates for the NRF plots are shown in Figure 8. Based on the LOWESS trend lines, understory density did not pose a large visibility bias in this study. Except for a single plot with very high understory density (> 30000 trees per ha), the trend lines remained around 15 m^2/ha, indicating little impact of understory density on FBA. The value of 15 is very close to the intercept coefficient estimated above (Tab. 2), and the results here show that the variation in FBA - PBA (Fig. 8) was not due to understory vegetation.

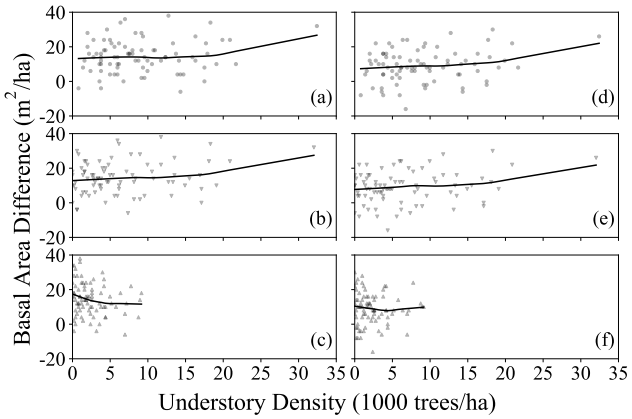

Figure 8: Effects of understory density on the basal area difference (field basal area – photo basal area, m^2/ha) in the NRF plots as determined by two marking methods (target counting (left panels) versus edge marking (right panels)). (a) and (d) are total understory trees, (b) and (e) are understory trees whose height smaller than 1.3 m, while (c) and (f) are those understory trees greater than 1.3 m.

4 Discussion

Our results show that spherical images from a consumer-grade 360° camera can efficiently and effectively estimate basal area using photo-based angle-count sampling. While underestimation was consistently observed, the trend did not appear to be related to amount of basal area per ha present, understory vegetation, nor inter-user variability. As a result, underestimation could be easily corrected using some form of double sampling (Dai, 2018; Dick, 2012) with ratio correction.

In this study, two photo processing methods were used: the edge marking method and the octagon target counting method. The resulting PBA estimates were acceptable for both methods. The advantage of edge

marking was that different BAFs can be assessed without re-marking, but this is generally only useful for big BAF sampling (Bell et al., 1983; Iles, 2003; Marshall et al., 2004) or for research situations where one is interested in effects of different BAFs (as in this study). All users in this study felt the target counting was more familiar (more similar to the process they used in the field) and more repeatable than edge marking. Difficulties recognizing tree edges, especially in dense forest conditions, along with twice the number of mouse clicks for each tree, could potentially cause higher user errors. The octagon target count method avoided potential edge marking errors and only required one click; however, repeated marking for different BAFs would be required.

It was expected that visibility bias would increase with increasing basal area because of an increasing number of hidden trees; This was not observed in this study. There are several potential explanations for this result. First, and most likely, the results obtained here were the compensatory effects of underestimation caused by hidden trees coupled with overestimation caused by increased user error as field basal area increased. In this study, the plots with the highest basal areas were generally composed of very dense small stems, especially on the NL sites. With many small trees in an image it can be difficult to distinguish multiple overlapping small trees from one larger individual tree. With the edge marking method, it can be very difficult to clearly see the tree edges due to the resolution and exposure conditions (Fig. 7.b). Secondly, the plots with very high basal areas also had a significant number of dead trees present. While care was exercised in determining live/dead trees and in avoiding marking dead trees, this could have increased counts on the higher basal area plots. Both factors may have also contributed to the lack of improvement in PBA estimates with increasing BAF.

Multiple digital sampling locations within plots greatly decreased effects of hidden trees and any user errors. In several individual images there were nearby tree trunks which occluded large portions of the plot radial view. The potential for hidden trees in these situations was quite large. The multiple digital sample locations minimize this issue by providing multiple plot viewpoints, as well as capturing more of the local spatial variability. Hidden trees cannot be observed using any remote sensing technique and represent a difficult problem to deal with (Ducey et al., 2013, 2011; Zasada et al., 2013). When carrying out field measured angle count sampling, it is possible for the observer to lean left and right or even to slightly change their location to identify hidden trees. Distances from plot center and diameters of hidden trees also can be measured to determine if hidden trees are count trees or not. This is not possible with photographic or other remote sensing methods (Fastie, 2010). Building a model to correct for hidden tree effects can be very complex and should take into account stand density, distance from tree to sensor, the thickness of each tree trunk, and so on (Zasada et al., 2013). Such model-based approaches are inherently more variable and require substantial field data to calibrate (Ducey et al., 2013). A simpler method is to use double sampling with ratio correction (Dai, 2018; Dick, 2012) or some form of distance sampling correction (Kershaw, 2010). We have shown another alternative, which is to simply add additional digital sampling locations within a plot, which is often the solution employed with terrestrial LiDAR scanning (Seidel et al., 2012; Wallace et al., 2017). Limiting plot size (or in this case increasing BAF) is another way to decrease effects of hidden trees (Dick, 2010; Zasada et al., 2013); however, this did not seem to be effective in this study. While multiple digital sample locations improve PBA estimation, it greatly increases field acquisition time. Given that angle count sampling is already an efficient method to implement in the field, multiple images would likely require more field effort. Double sampling with ratio correction is most likely to be the most efficient method for dealing with hidden trees (Dai, 2018; Dick, 2012).

It is very important to determine an appropriate BAF for angle-count sampling (Bitterlich, 1984; Iles, 2003; Yang et al., 2017). Choice of BAF greatly influences variability, which in turn, influences sample size requirements, numbers of trees counted per plot, and ultimately inventory costs (Iles, 2012; Yang et al., 2017). We found that BAF could be increased to about 5 without substantially increasing variability. Yang et al. (2017) obtained similar results for the entire NRF. The increased BAF had the added effect of slightly reducing visibility bias; thus a trade-off between visibility bias and plot variation needs to be considered when implementing photo-based angle count sampling.

In this study, understory vegetation did not seem to influence visibility bias. Concerns about effects of understory vegetation has been mentioned by many photo-based forest inventory studies (Dick, 2010; Fastie, 2010; Perng et al., 2018; Stewart, 2004), but none of these studies verified this effect experimentally. We found that different understory tree densities had no significant impact on the differences between FBA and PBA. This was contrary to our expectations. A possible explanation for this phenomenon is that most of the understory vegetation in the study plots were shorter than 1.3 m in height. Additional advantages in our study include very flat terrain and the ability to view up the stem and visualize stem size when taller understory vegetation blocked the view.

Variability between different users is a very important consideration when choosing measurement meth-

ods. While a few photo forest mensuration studies have shown that they can achieve small differences between field measured data and photo measured data (Clark et al., 2000; Fastie, 2010; Rodríguez-García et al., 2014), none, to our knowledge, have systematically tested the repeatability and reproducibility among different users. Our repeatability test, given by seven volunteers, showed: (1) Random effects of image processing order (familiarity of software) and different users did not have significant impacts on photo estimation; (2) the denser the plot, the more differences between users due to manual identification and selection by mouse clicking; and (3) using octagon target counts did not require identifying tree edges and resulted in lower underestimation than edge marking.

Many studies have focused on individual tree measurements, before summarizing these measures into stand level attributes. Some studies use scale tags placed on each tree or measured field distances and slopes (Dick, 2010; Lu et al., 2019). These methods require measuring or tagging individual trees, which is time-consuming and costly and/or requires multiple images for each tree of interest (Perng et al., 2018; Stewart et al., 2004). These techniques have limited benefit for improving inventory efficiency. In addition, errors resulting from stitching several digital photos together cannot be avoided (Dick, 2010; Fastie, 2010; Lu et al., 2019; Perng et al., 2018). Structure from Motion (SfM) is an "automatic" merging technology which enables 3D reconstruction from photo series without actual measurements (Fang and Strimbu, 2017; Sanvely et al., 2008). Several studies have used this technique to reconstruct individual tree stems (Miller et al., 2015; Mokroš et al., 2018; Surový et al., 2016), or to develop stand level point clouds (Forsman et al., 2016; Liang et al., 2014, 2015; Liu et al., 2018). However, this automatic technology requires obtaining a large number of photos (Berveglieri et al., 2017a; Liu et al., 2018) and high performance computers and complex algorithms to conduct analysis (Belton et al., 2013; Liang et al., 2015; Mulverhill et al., 2019). In addition, the point clouds require subsequent measurement to produce the tree and stand attributes. Our method simply extracts the stand-level basal area directly from the photos.

The method we have proposed here has several advantages. First, using a consumer-grade spherical camera is a very cost-effective (around $400 CDN) and time-efficient (less than 1 minute per photo) method. The produced image is automatically merged into the camera, eliminating the often time-consuming task of acquiring and stitching multiple photos from different view radii (Dick, 2010; Fastie, 2010) or placing reference scale objects in the field (Dean, 2003; Perng et al., 2018; Varjo et al., 2006). Keeping permanent digital records for forest plots provides the opportunity for making new retrospective measurements. This aspect is likely to become more advantageous as novel technology develops in the future (Iles, 1994). Finally, quantification of differences among users is difficult to assess and correct with most field measurement techniques. The software developed here keeps a record of individual markings (Fig. 7) that could be used as a comparison reference for correcting photo-based samples.

This study also had some limitations. The camera elevation was not exactly at the definition of breast height (1.3 m). When selecting tree trunks for marking and estimating basal area at breast height, we used the equatorial plane of the spherical camera rather than calculating 1.3 m height on tree trunks based on stereoscopic principles (Perng et al., 2018; Rodríguez-García et al., 2014; Sánchez-González et al., 2016). Also, merging two hemispherical lenses into spherical image sometimes caused the joint region fuzzy or blurred, makes tree trunk identification more difficult. Variable sunlight conditions can result in inconsistent exposure levels across the spherical image. Underexposure makes trunks in the far distance dark and hard to distinguish while overexposure flashes out trunk edges. Our terrain was relatively flat. In steeper terrain, different methods for identifying breast height on trees will be required. This is a more complicated problem than is currently implementing in our lab. Finally, all images were marked manually, which is time consuming and prone to user error. Automatic image processing and 3D reconstruction is a rapidly developing area (Hapca et al., 2007). It may prove feasible to automatize the process described here by applying computer vision and developing algorithms similar to our manual selection methods (Berveglieri et al., 2017b; Sánchez-González et al., 2016). Another possibility is to use Structure from Motion (SfM) techniques (Sanvely et al., 2008) to obtain point clouds from different camera views (Forsman et al., 2016; Liang et al., 2014; Mokroš et al., 2018; Surový et al., 2016); however, as mentioned above, point cloud development obviates the simplicity of the methods developed here – other than clicking trees, no measurements were required. Last but not least, as Iles (2018) pointed out, using attributes easily obtained by novel technologies (lead by LiDAR) to build models to avoid messy field inventory may be tempting. But using sample to correct initial estimate rather than creating a correction model is still important.

5 Conclusion

Spherical photos are suitable for estimating stand basal area based on modified angle-count sampling methods. Adding multiple digital sample locations can decrease effects of visibility bias. Careful selection of

BAF can somewhat reduce visibility bias without substantially increasing variation. Variability among different users did not seem to be a significant problem in implementing photo angle counts. Though limited by occasionally fuzzy joint regions and extreme sunlight conditions, this novel method could still be a cost-effective and efficient method to increase field sample sizes and to provide permanent forest records for future use. Effects of understory vegetation and sloping terrain needs to be examined beyond the range of conditions encountered in this study. Future research should focus on other forest attribute extraction, such as height and diameter and automatic image processing.

6 Acknowledgements

Funding for this project was provided in part by the National Science and Engineering Research Council of Canada Discovery Grants program, the Province of Newfoundland and Labrador Centre for Forest Science and Innovation Contribution Agreement, and the New Brunswick Innovation Foundation Research Assistants Initiative and Graduate Scholarships programs. The authors also thank the labmates, collaborators, and summer field crew who helped make this project possible: Emily Loretta Nicholson, UNB; Dr. Mike Lavigne, Gretta Goodine, and Rodney Foster, Atlantic Forestry Research Centre, Natural Resources Canada; We also thank Yang Zhan, Wushuang Li, Shun-Ying Chen, and Yunjia Dai for their volunteer work in software testing and inter-observer error analysis.

References

Baskerville, G. 1986. Understanding forest management. Forestry Chronicle 62:339–347. at: https://www.doi.org/10.5558/tfc62339-4.

Bell, J. F., K. Iles, and D. Marshall. 1983. Balancing the ratio of tree count-only sample points and VBAR measurements in variable plot sampling. Pages 699–702 Bell J.F. and Atterbury, T. (eds.). Proceedings: Renewable Resource Inventories for Monitoring Changes and Trends. College of Forestry, Oregon State University, Corvallis, OR. at: https://www.osti.gov/biblio/6295064.

Belton, D., S. Moncrieff, and J. Chapman. 2013. Processing tree point clouds using Gaussian Mixture Models. Pages 43–48 ISPRS Annals of Photogrammetry, Remote Sensing and Spatial Information Sciences. Copernicus GmbH, Antalya, Turkey. at: https://www.doi.org/10.5194/isprsannals-II-5-W2-43-2013.

Berveglieri, A., A. Tommaselli, X. Liang, and E. Honkavaara. 2017a. Photogrammetric measurement of tree stems from vertical fisheye images. Scandinavian Journal of Forest Research 32:737–747. at: https://doi.org/10.1080/02827581.2016.1273381.

Berveglieri, A., A. M. G. Tommaselli, X. Liang, and E. Honkavaara. 2017b. Vertical Optical Scanning with Panoramic Vision for Tree Trunk Reconstruction. Sensors 17(2791). at: https://www.doi.org/10.3390/s17122791.

Bettinger, P., K. Boston, J. Siry, and D. Grebner. 2017. Forest Management and Planning. 2nd edn. Academic Press, San Diego, CA. at: https://books.google.ca/books?id=cHnUDAAAQBAJ.

Bitterlich, W. 1947. Die winkelzählmessung (Measurement of basal area per hectare by means of angle measurement.). Allgemeine Forst- und Holzwirtschaftliche Zeitung 58:94–96.

Bitterlich, W. 1984. The relascope idea: Relative measurements in forestry. First. CAB International, Slough, England. at: https://academic.oup.com/forestscience/article/32/1/35/4642254.

Chazdon, R. L. 2008. Beyond Deforestation: Restoring Forests and Ecosystem Services on Degraded Lands. Science 320:1458–1460. at: https://www.doi.org/10.1126/science.1155365.

Christensen, N. L., A. M. Bartuska, J. H. Brown, S. Carpenter, C. D'Antonio, R. Francis, J. F. Franklin, J. A. MacMahon, R. F. Noss, D. J. Parsons, C. H. Peterson, M. G. Turner, and R. G. Woodmansee. 1996. The report of the Ecological Society of America committee on the scientific basis for ecosystem management. Ecological Applications 6:665–691. at: https://doi.org/10.2307/2269460.

Clark, N. A., R. H. Wynne, D. L. Schmoldt, and M. Winn. 2000. An assessment of the utility of a non-metric digital camera for measuring standing trees. Computers and Electronics in Agriculture 28:151–169. at: https://www.doi.org/10.1016/S0168-1699(00)00125-3.

Clutter, J. L., J. C. Fortson, L. V. Pienaar, G. H. Brister, and R. L. Bailey. 1983. Timber management. A quantitative approach. First. John Wiley & Sons, New York. at: https://www.cabdirect.org/cabdirect/abstract/19840691762.

Dai, X. 2018. Bias correction in panoramic photo-based angle count sampling. Unpub. BScF Honors, University of New Brunswick, Fredericton, NB, Canada.

Dean, C. 2003. Calculation of wood volume and stem taper using terrestrial single-image close-range photogrammetry and contemporary software tools. Silva Fennica 37:359–380. at: https://pdfs.semanticscholar.org/88c6/aa57bbd892c373e1da5ef4567cc510c9c786.pdf.

DeCourt, N. 1956. Utilisation de la photographie pour mesurer les surfaces terrières (The use of photography for measuring basal area). Revue Forestière Française 8:505–507. at: http://documents.irevues.inist.fr/bitstream/handle/2042/27219/RFF_1956_7_505.pdf.

Dick, A. R. 2012. Forest inventory using a camera: Concept, field implementation and instrument development. Unpublished MScF Thesis, University of New Brunswick, Fredericton, NB, Canada.

Dick, A. R., J. A. Kershaw, and D. A. MacLean. 2010. Spatial Tree Mapping Using Photography. Northern Journal of Applied Forestry 27:68–74. at: https://www.doi.org/10.1093/njaf/27.2.68.

Ducey, M. J., and R. Astrup. 2013. Adjusting for non-detection in forest inventories derived from terrestrial laser scanning. Canadian Journal of Remote Sensing 39:410–425. at: https://www.tandfonline.com/doi/full/10.5589/m13-048.

Ducey, M. J., and J. A. Kershaw. 2011. Vertical Point Sampling with a Camera. Northern Journal of Applied Forestry 28:61–65. at: https://www.doi.org/10.1093/njaf/28.2.61.

Fang, R., and B. Strimbu. 2017. Photogrammetric point cloud trees. Mathematical and Computational Forestry & Natural Resource Sciences 9:30–33. at: http://www.mcfns.net/index.php/Journal/article/view/9.8.

Fastie, C. L. 2010. Estimating stand basal area from forest panoramas. Page 8 Proceedings of the Fine International Conference on Gigapixel Imaging for Science. Carnegie Mellon University, Pittsburg, PA. at: https://kilthub.cmu.edu/articles/Estimating_stand_basal_area_from_forest_panoramas/6709391/1.

Forsman, M., N. Börlin, and J. Holmgren. 2016. Estimation of Tree Stem Attributes Using Terrestrial Photogrammetry with a Camera Rig. Forests 7(61). at: https://www.doi.org/10.3390/f7030061.

Gillis, A. M. 1990. The New Forestry. BioScience 40:558–562. at: https://doi.org/10.2307/1311294.

Grosenbaugh, L. R. 1952. Plotless timber estimates–New, fast, easy. Journal of Forestry 50:32–37. at: https://www.doi.org/10.1093/jof/50.1.32.

Grosenbaugh, L. R. 1958. Point-sampling and line-sampling: Probability theory, geometric implications, synthesis. Page 34. Occasional Paper, USDA Forest Service, Southern Forest Experiment Station. at: https://www.fs.usda.gov/treesearch/pubs/2458.

Grosenbaugh, L. R. 1963. Optical dendrometers for out-of-reach diameters: A conspectus and some new theory. Forest Science Monographs 4(48). at: https://doi.org/10.1093/forestscience/9.s2.a0001.

Guido, van R. 2018. Python (programming language). Python Software Foundation, US. Last Accessed 12-11-2018. at: https://docs.python.org/3.6/reference/index.html.

Hapca, A. I., F. Mothe, and J.-M. Leban. 2007. A digital photographic method for 3D reconstruction of standing tree shape. Annals of Forest Science 64:631–637. at: http://www.doi.org/10.1051/forest:2007041.

Husch, B. 1980. How to determine what you can afford to spend on inventories. Pages 98–102 IUFRO Workshop on Arid Land Resource Inventories. USDA, Forest Service, Washington Office, General Technical Report WO-28, La Paz, Mexico. at: https://www.cabdirect.org/cabdirect/abstract/19822611128.

Iles, K. 1994. Directions in Forest Inventory. Journal of Forestry 92:12–15. at: https://www.doi.org/10.1093/jof/92.12.12.

Iles, K. 2003. A sampler of inventory topics. 2nd edition. Kim Iles and Associates, Nanaimo, BC. at: https://books.google.ca/books/about/A_Sampler_of_Inventory_Topics.html?id=sGDlAAAACAAJ.

Iles, K. 2012. Some Current Subsampling Techniques in Forestry. Mathematical & Computational Forestry & Natural Resource Sciences 4(2). at: http://mcfns.net/index.php/Journal/article/view/143/MCNFS-4.2_77.

Iles, K. 2018. Are Models the Answer? Mathematical and Computational Forestry & Natural-Resource Sciences (MCFNS) 10:6-8(3). at: https://mcfns.net/index.php/Journal/article/view/10.2.

Jenkins, J. C., D. C. Chojnacky, L. S. Heath, and R. A. Birdsey. 2003. National scale biomass estimators for United States tree species. Forest Science 49:12–35.

at: https://www.fs.usda.gov/treesearch/pubs/6996.

Kershaw, J. A., Jr. 2010. Correcting for visibility bias in photo point samples. Northeastern Mensurationists Organization Annual Meeting, Stockbridge, MA.

Kershaw, J. A., Jr., M. J. Ducey, T. W. Beers, and B. Husch. 2016. Forest Mensuration. 5th edition. Wiley/Blackwell, Hobokin, NJ. at: https://books.google.ca/books?id=ymhxDQAAQBAJ.

Lambert, M.-C., C.-H. Ung, and F. Raulier. 2005. Canadian national tree aboveground biomass equations. Canadian Journal of Forest Research 35:1996–2018. at: https://doi.org/10.1139/x05-112.

Liang, X., A. Jaakkola, Y. Wang, J. Hyyppä, E. Honkavaara, J. Liu, and H. Kaartinen. 2014. The Use of a Hand-Held Camera for Individual Tree 3D Mapping in Forest Sample Plots. Remote Sensing 6:6587–6603. at: https://www.doi.org/10.3390/rs6076587.

Liang, X., Y. Wang, A. Jaakkola, A. Kukko, H. Kaartinen, J. Hyyppä, E. Honkavaara, and J. Liu. 2015. Forest Data Collection Using Terrestrial Image-Based Point Clouds From a Handheld Camera Compared to Terrestrial and Personal Laser Scanning. IEEE Transactions on Geoscience and Remote Sensing 53:5117–5132. at: https://www.doi.org/10.1109/TGRS.2015.2417316.

Liu, J., Z. Feng, L. Yang, A. Mannan, T. U. Khan, Z. Zhao, and Z. Cheng. 2018. Extraction of Sample Plot Parameters from 3D Point Cloud Reconstruction Based on Combined RTK and CCD Continuous Photography. Remote Sensing 10(1299). at: https://www.doi.org/10.3390/rs10081299.

Lootens, J. R., D. R. Larsen, and S. R. . Shifley. 2007. Height-diameter equations for 12 upland species in the Missouri Ozark Highlands. Northern Journal of Applied Forestry 24:1149–1152. at: https://www.doi.org/10.1093/njaf/24.2.149.

Lu, M.-K., T. Y. Lam, B.-H. Perng, and H.-T. Lin. 2019. Close-range photogrammetry with spherical panoramas for mapping spatial location and measuring diameters of trees under forest canopies. Canadian Journal of Forest Research 49:865–874. at: https://www.doi.org/10.1139/cjfr-2018-0430.

Marshall, D. D., K. Iles, and J. F. Bell. 2004. Using a large-angle gauge to select trees for measurement in variable plot sampling. Canadian Journal of Forest Research 34:840–845. at: https://doi.org/10.1139/x03-240.

Miller, J., J. Morgenroth, and C. Gomez. 2015. 3D modelling of individual trees using a handheld camera: Accuracy of height, diameter and volume estimates. Urban Forestry & Urban Greening 14:932–940. at: https://www.doi.org/10.1016/j.ufug.2015.09.001.

Mokroš, M., J. Výboštok, J. Tomaštík, A. Grznárová, P. Valent, M. Slavík, and J. Merganič. 2018. High Precision Individual Tree Diameter and Perimeter Estimation from Close-Range Photogrammetry. Forests 9(696). at: https://www.doi.org/10.3390/f9110696.

Mulverhill, C., N. C. Coops, P. Tompalski, C. W. Bater, and A. R. Dick. 2019. The utility of terrestrial photogrammetry for assessment of tree volume and taper in boreal mixedwood forests. Annals of Forest Science 76(83). at: https://www.doi.org/10.1007/s13595-019-0852-9.

Opie, J. E. 1968. Predictability of Individual Tree Growth Using Various Definitions of Competing Basal Area. Forest Science 14:314–323. at: https://www.doi.org/10.1093/forestscience/14.3.314.

Pan, Y., R. A. Birdsey, O. L. Phillips, and R. B. Jackson. 2013. The Structure, Distribution, and Biomass of the World's Forests. Annual Review of Ecology, Evolution, and Systematics 44:593–622. at: https://www.doi.org/10.1146/annurev-ecolsys-110512-135914.

Perng, B.-H., T. Y. Lam, and M.-K. Lu. 2018. Stereoscopic imaging with spherical panoramas for measuring tree distance and diameter under forest canopies. Forestry: An International Journal of Forest Research 91:662–673. at: https://www.doi.org/10.1093/forestry/cpy028.

Ricoh Imaging Company, LTD. 2016. Rioch Theta S 360 video camera. Last Accessed 26-08-2016. at: http://www.ricoh-imaging.co.jp/english/products/theta_s/.

Rodríguez-García, C., F. Montes, F. Ruiz, I. Cañellas, and P. Pita. 2014. Stem mapping and estimating standing volume from stereoscopic hemispherical images. European Journal of Forest Research 133:895–904. at: https://www.doi.org/10.1007/s10342-014-0806-6.

Rowe, J. S. 1972. Forest Regions of Canada. Publication, Fisheries and Environment Canada, Canadian Forest Service, Headquarters, Ottawa. 172 p. at: https://cfs.nrcan.gc.ca/publications?id=24040.

Sánchez-González, M., M. Cabrera, P. J. Herrera, R. Vallejo, I. Cañellas, and F. Montes. 2016. Basal Area and Diameter Distribution Estimation Using Stereoscopic Hemispherical Images. Photogrammetric Engineering & Remote Sensing 82:605–616. at: https://www.doi.org/10.14358/PERS.82.8.605.

Seidel, D., S. Fleck, and C. Leuschner. 2012. Analyzing forest canopies with ground-based laser scanning: A comparison with hemispherical photography. Agricultural and Forest Meteorology 154–155:1–8. at: https://www.doi.org/10.1016/j.agrformet.2011.10.006.

Slik, J. W. F., S.-I. Aiba, F. Q. Brearley, C. H. Cannon, O. Forshed, K. Kitayama, H. Nagamasu, R. Nilus, J. Payne, G. Paoli, A. D. Poulsen, N. Raes, D. Sheil, K. Sidiyasa, E. Suzuki, and J. L. C. H. van Valkenburg. 2010. Environmental correlates of tree biomass, basal area, wood specific gravity and stem density gradients in Borneo's tropical forests. Global Ecology and Biogeography 19:50–60. at: https://www.doi.org/10.1111/j.1466-8238.2009.00489.x.

Snavely, N., S. M. Seitz, and R. Szeliski. 2008. Modeling the World from Internet Photo Collections. International Journal of Computer Vision 80:189–210. at: https://www.doi.org/10.1007/s11263-007-0107-3.

Stewart, B. 2004, August. Using a camera as an angle gauge in angle-count sampling. MF Thesis, The University of Georgia. at: http://athenaeum.libs.uga.edu/handle/10724/21991.

Stewart, B., C. J. Cieszewski, and M. Zasada. 2004. Use of a camera as an angle-gauge in angle-count sampling. Pages 375–380 Second International Conference on Forest Measurements and Quantitative Methods and Management. Warnell School of Forestry and Natural Resources, University of Georgia, Athens, GA. at: https://www.fs.fed.us/pnw/olympia/silv/publications/opt/491_MarshallEtal2004.pdf.

Surový, P., A. Yoshimoto, and D. Panagiotidis. 2016. Accuracy of Reconstruction of the Tree Stem Surface Using Terrestrial Close-Range Photogrammetry. Remote Sensing 8:123. at: https://www.doi.org/10.3390/rs8020123.

Varjo, J., H. Henttonen, J. Lappi, J. Heikkonen, and J. Juujärvi. 2006. Digital horizontal tree measurements for forest inventory. Working papers of the Finnish Forest Research Institute 40(23). at: http://jukuri.luke.fi/handle/10024/535955.

Wallace, L., S. Hillman, K. Reinke, and B. Hally. 2017. Non-destructive estimation of above-ground surface and near-surface biomass using 3D terrestrial remote sensing techniques. Methods in Ecology and Evolution 8:1607–1616. at: https://www.doi.org/10.1111/2041-210X.12759.

Weiskittel, A. R., D. W. Hann, J. A. Kershaw Jr., and J. K. Vanclay. 2011. Forest Growth and Yield Modeling. 2nd edition. Wiley/Blackwell, New York. at: https://www.wiley.com/en-us/Forest+Growth+and+Yield+Modeling-p-9780470665008.

Yang, T.-R., Y.-H. Hsu, J. A. Kershaw, E. McGarrigle, and D. Kilham. 2017. Big BAF sampling in mixed species forest structures of northeastern North America: influence of count and measure BAF under cost constraints. Forestry: An International Journal of Forest Research 90:649–660. at: https://www.doi.org/10.1093/forestry/cpx020.

Zar, J. H. 2009. Biostatistical analysis. 5th edition. Pearson, New York. at: https://www.pearson.com/us/higher-education/product/Zar-Biostatistical-Analysis-5th-Edition/9780131008465.html.

Zasada, M., K. Stereńczak, W. M. Dudek, and A. Rybski. 2013. Horizon visibility and accuracy of stocking determination on circular sample plots using automated remote measurement techniques. Forest Ecology and Management 302:171–177. at: https://www.doi.org/10.1016/j.foreco.2013.03.041.